JOURNAL OF MATERIALS SCIENCE 25 (1990) 1275–1284

Development of a new 304L austenitic welding consumable containing tungsten

J. J. SMITH*, C. PERRY, R. A. FARRAR
Department of Mechanical Engineering, The University of Southampton, Hampshire, UK

The transformation behaviour and kinetics of a duplex weld metal, in which tungsten was substituted for molybdenum, have been studied at 600, 700 and 800° C. Despite a low carbon level (0.037 wt %), the material exhibited exceptional resistance against intermetallic formation during ageing. The Charpy impact toughness at room temperature was consistently superior compared to a standard molybdenum containing 316 weld metal. The results suggest that suitable development of the tungsten-bearing 304 consumable could lead to significant improvements in weld-metal properties.

1. Introduction

Austenitic stainless steels have been widely used in conventional and nuclear power plant for applications such as superheater and header components. The wrought steels have good ductility and toughness over a wide range of temperature and exhibit excellent corrosion and oxidation resistance. In any such installation, welded joints are critical load-bearing components and it is important that their properties do not deteriorate during post-weld heat treatment or at service temperatures.

AISI type 316 steel is generally welded with either a consumable of approximately matching composition to the base material 19Cr–12Ni–2Mo, or with a leaner 17Cr–8Ni–2Mo alloy. The composition of the weld metal is controlled to produce a small amount of δ-ferrite in the deposit, 3 to 8%, to prevent hot cracking. However, it has been found that during post-weld heat treatment or high-temperature service ($\sim 550°$ C), the δ-ferrite can transform to $M_{23}C_6$ carbides and/or intermetallic σ and χ phases which can seriously degrade the mechanical properties [1, 2]. Studies by Farrar [3] and more recently by Smith [4] on 17Cr–8Ni–2Mo weld metals have shown that a bulk carbon level of 0.07 wt % is required to prevent excessive intermetallic formation. It has been shown that the precipitation of $M_{23}C_6$ carbides at the δ–γ boundaries denudes the δ-ferrite of chromium and molybdenum and lower its propensity to transform to intermetallic phases.

However, Smith [14] has shown that the bulk carbon level must be accurately controlled, since carbon levels in excess of 0.09 wt % can result in excessive grain boundary carbide formation, which embrittles the weld metal. In addition, for certain applications a carbon level of 0.07 wt % may be unacceptable due to the possible sensitization of the weld metal during fabrication. In the present work, it was proposed to substitute molybdenum with various levels of tungsten in the weld metal. The use of tungsten as an alloying addition in duplex weld metals and its effect on microstructural transformation behaviour have not been previously investigated. Wegrzyn and Klimpel [5] and Hull [6] have both reported that wrought stainless steels containing tungsten have a lower propensity to form intermetallics σ and χ than steels containing similar amounts of molybdenum. Consequently, in the present investigation it was hoped that the tungsten-containing weld deposits would exhibit better long-term resistance to intermetallic formation and superior room-temperature toughness compared to the standard 17Cr–8Ni–2Mo weld metal.

2. Experimental procedure

2.1. Materials

The weld metals were deposited by the manual metal arc (MMA) process employing 4 mm electrodes with rutile coatings. The welds were deposited in the downhand position at 115 A d.c. (electrode positive). The welds were laid down as butt joints with a 10° angle preparation and were produced with approximately 25 weld passes. Standard Charpy blanks were machined from each weld such that the specimen axes were normal to the grain orientation. The chemical analyses of the weld metals and the as-deposited δ-ferrite contents are shown in Table I. The deposits were designed to have low and intermediate carbon levels and were designated 304 LW and 304 W, respectively. BW15 is a standard 17Cr–8Ni–2Mo type weld metal. This material is currently in commercial service and is thought to be one of the best material available in terms of its transformation behaviour and mechanical properties. Although BW15 has been previously studied by Farrar *et al.*, [7], it has been included in order that direct comparisons can be made between the weld-metal deposits.

* *Present address*: IPTME, Loughborough University of Technology, LE11 3TU, UK.

0022–2461/90 $03.00 + .12

TABLE I Chemical analysis and as-deposited ferrite levels

Specimen	Composition (wt %)															
	Cr	Ni	Mo	W	C	Mn	Si	P	Al	Nb	V	O*	N*	Cr_{eq}†	Ni_{eq}†	Initial ferrite
304LW	17.63	9.13	< 0.02	1.7	0.037	2.12	0.4	0.02	< 0.002	0.04	0.08	790	857	19.9	13.9	4.6
304W	17.81	9.13	< 0.02	3	0.064	2.14	0.4	0.02	< 0.002	0.04	0.09	655	590	21.35	13.9	4.7
BW15	16.9	9.1	1.55	-	0.065	1.8	0.29	0.019	< 0.003	0.009	0.02	640	400	20.1	13.15	4.6

*Analysis as p.p.m.
†Hull equivalent $Cr_{eq} = Cr + 1.58\,Si + 1.76\,Mo + 0.97\,W$; $Ni_{eq} = Ni + 0.5\,Mn + 30\,C + 30\,N$.

2.2. δ-Ferrite transformation

The δ-ferrite contents of the as-deposited and aged specimens were determined using a Magne-Gage magnetic measuring instrument. This was calibrated with primary and secondary standards according to the AWS A4-2-74 procedure. In order to minimize error, a template of the Charpy specimen was placed on the surface to ensure that the specimens were located in precisely the same position relative to the magnetic probe before and after heat treatment. Readings were made at eight different locations on the Charpy specimens (two per face), which were numbered so that the precise change in the δ-ferrite content could be calculated.

2.3. Heat treatment

The specimens were encapsulated in silica tubes, sealed in argon under a pressure of 0.333 atm and aged in horizontal tube furnaces between 600 and 800° C. The specimens were aged for times up to 3000 h.

2.4. Specimen preparation and examination

Standard 10 mm × 10 mm × 55 mm Charpy "V" impact specimens were machined from the butt joint, with the columnar grains perpendicular to the specimen axis.

A number of different etchants were used to examine the microstructure, including modified Murakami's reagent (30 g KOH, 30 g $Fe(CN)_6$ in 100 ml H_2O, 5 to 15 sec at 95° C), and electrolytic etches, nitric acid (60 ml HNO_3, 40 ml H_2O at 0.4 V cm^{-2}) and oxalic acid (10 g oxalic acid, 100 ml H_2O at 0.6 V cm^{-2}). The specimens were examined using optical, scanning and transmission electron microscopy.

Extraction replicas and foils were examined in a Jeol 100CX scanning transmission electron microscope with STEM and energy-dispersive X-ray (EDX) analysis facilities.

3 mm diameter rods were machined from the as-welded and aged specimens. After slicing and mechanical polishing to a thickness of 110 to 130 μm, the discs were electropolished using a solution of 5% perchloric in acetic acid, using conditions of 200 mA at a potential of 73 V.

3. Results

3.1. Isothermal transformation kinetics

The isothermal transformation curves for deposits

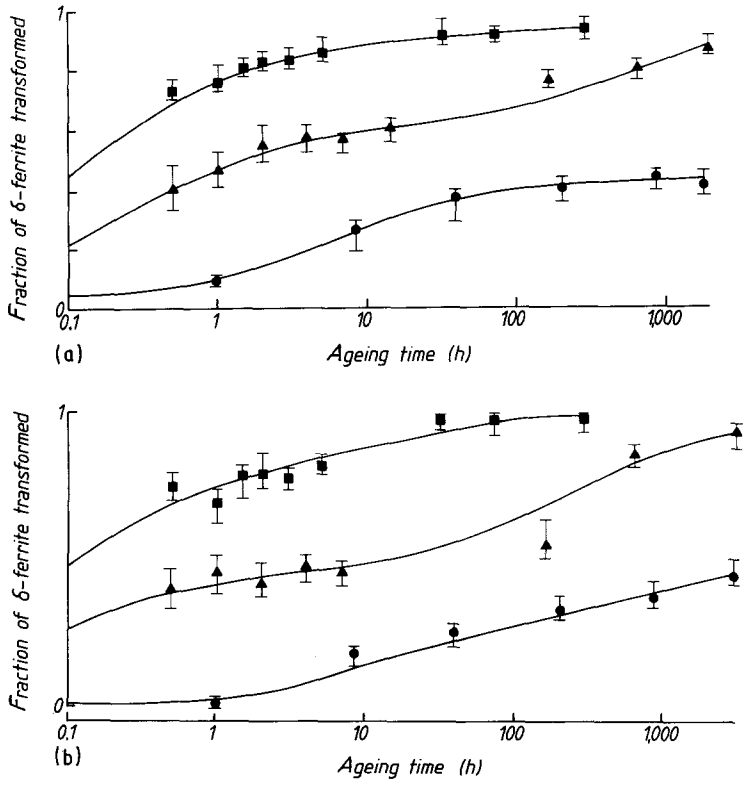

Figure 1 Fraction of δ-ferrite transformed on ageing at (●) 600, (▲) 700 and (■) 800° C, as a function of ageing time for (a) 304 LW and (b) 304 W. Error bars are also shown.

TABLE II Results of regression line fit of transformation data to Johnson–Mehl equation

T (°C)	n	b	Correlation coefficient r	Johnson–Mehl model
304LW				
600	0.208	0.151	0.89	$x = 1 - \exp(-0.151t^{0.208})$
700	0.153	0.634	0.99	$x = 1 - \exp(-0.634t^{0.153})$
800	0.121	1.525	0.96	$x = 1 - \exp(-1.525t^{0.121})$
304W				
600	0.407	0.035	0.87	$x = 1 - \exp(-0.035t^{0.407})$
700	0.172	0.506	0.91	$x = 1 - \exp(-0.506t^{0.172})$
800	0.231	1.332	0.97	$x = 1 - \exp(-1.332t^{0.231})$

304 LW and 304 W at 600, 700 and 800° C are shown in Figs 1a and b. The transformation curves were sigmodal in shape and could be modelled using the Johnson–Mehl equation

$$x = 1 - \exp(-bt^n) \quad (1)$$

where x is the δ-ferrite fraction transformed in time t, and b and n are constants.

The graphs of $\ln[-\ln(1 - x)]$ against $\ln t$ are approximately linear, which suggests that the Johnson–Mehl model is valid within the range of temperature studied. The values of b, n and the correlation coefficient r at each temperature were determined by linear regression analysis (Table II). The correlation coefficients are greater than 0.90 in most cases, indicating good linear correspondence. The fitting of these equations to the experimental data at 600, 700 and 800° C are shown in Figs 2a, b and c, respectively. These show a reasonable correlation between the experimental and theoretical behaviour.

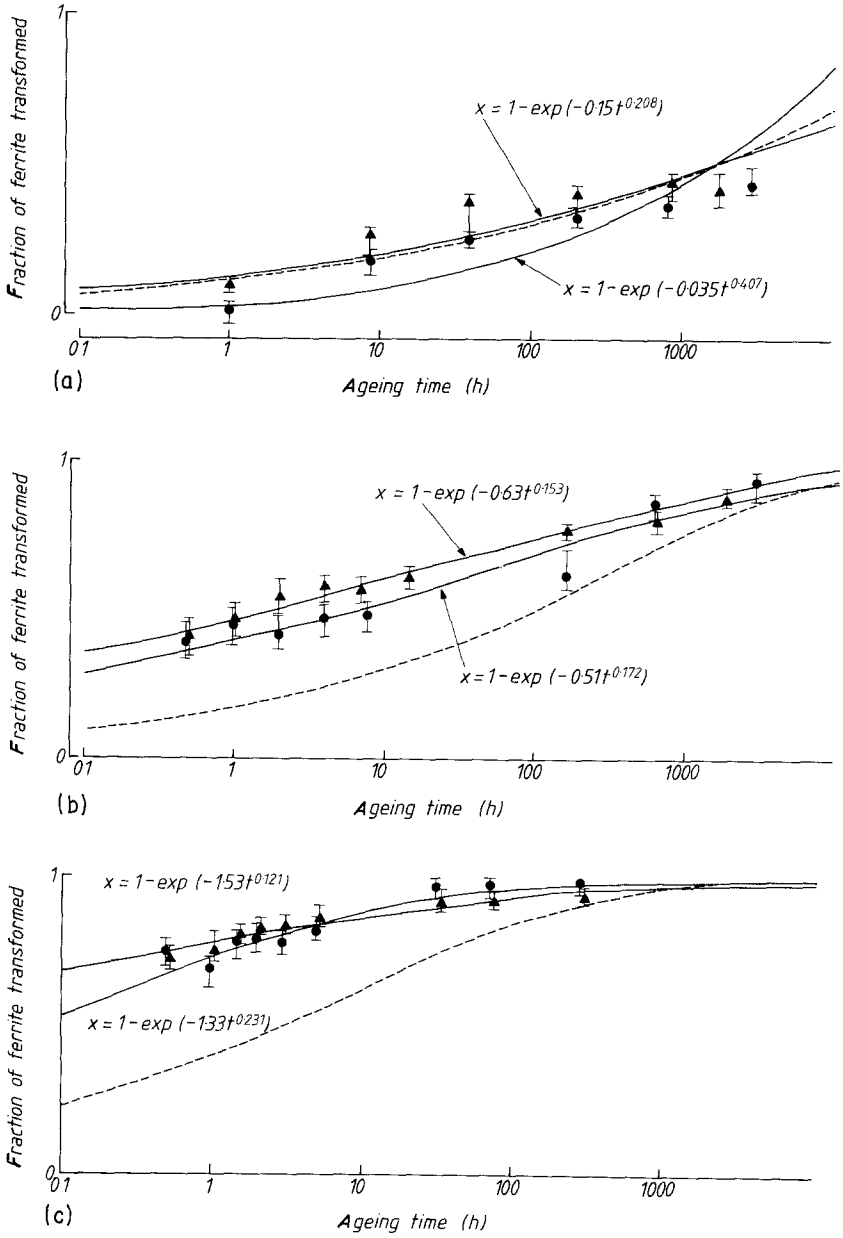

Figure 2 δ-ferrite transformation curves at (a) 600 (b) 700 and (c) 800° C. The curves have been fitted by least squares to the Johnson–Mehl equation $x = 1 - \exp(-bt^n)$. (▲) 304 LW, (●) 304 W, (– – –) BW15; error bars are also shown.

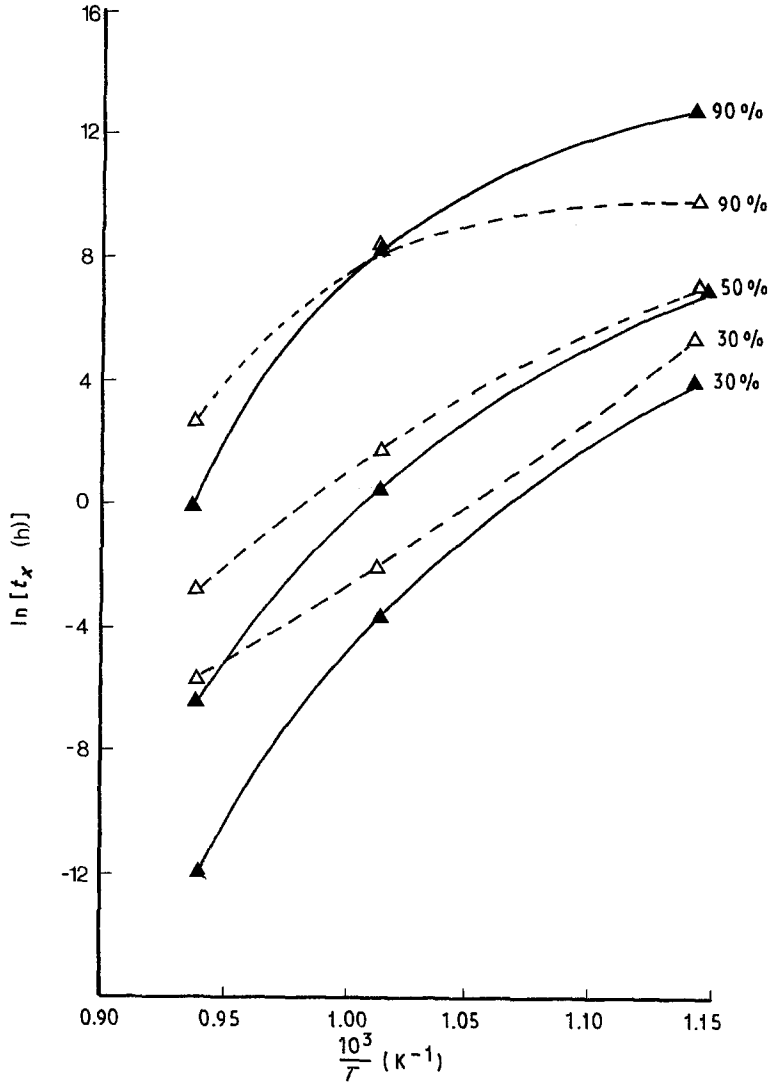

Figure 3 Temperature dependence of δ-ferrite transformation: (△) 304 LW, (▲) 304 W.

3.2. Temperature dependence of δ-ferrite transformation

Since n is nearly constant, the temperature dependence for the δ-ferrite transformation reaction can be modelled using the Arrhenius equation

$$\ln t = C - \ln A + \frac{E}{RT} \quad (2)$$

where t is the time for the reaction to proceed to a given transformation fraction, A is the Arrhenius constant, E is the apparent activation energy, R is the gas constant, T is the absolute temperature and C is a constant. If the experimental data are compatible with the Arrhenius equation then a plot of ln t against $1/T$ should yield a straight line of slope E/R and intercept $(C - \ln A)$. However, the relationship between the time for the reaction to proceed to a given fraction of δ-ferrite transformation (30, 50 and 90%) and the temperature is non-linear (Fig. 3). This implies that the activation energy for the dissolution of the δ-ferrite is not constant within the temperature range of study. It was therefore not possible to derive a general transformation equation relating time and temperature for weld metals 304LW and 304W.

3.3. Impact properties and fractography

The effect of ageing at 600, 700 and 800° C on the room-temperature impact toughness is shown in Figs 4a, b and c, respectively. At both 600 and 700° C, weld metals 304LW and 304W maintain a constant impact characteristic for times up to 3000 h. Examination of the fractures indicated that within the ageing times studied, the fractures were fully ductile. At higher ageing temperatures (800° C), after ageing in excess of 1000 h, both the tungsten-containing deposits showed a slight reduction in impact toughness. Examination of the fractures indicated that the fractures were predominantly ductile with small amounts of cleavage (Fig. 5).

At all ageing temperatures the impact values were significantly above those for the standard 17Cr–8Ni–2Mo weld metal (BW15).

3.4. Hardness

The effect of ageing time and temperature on the hardness of the deposits is shown in Fig. 6. At all temperatures, ageing resulted in an initial fall in the hardness. This was followed by a period during which the hardness remained nearly constant. After longer ageing times both deposits showed a small increase in hardness. The hardness values of the tungsten-containing deposits are comparable with those of the standard 17Cr–8Ni–2Mo deposit.

3.5. Metallography

3.5.1. As-welded microstructure

Weld metals 304LW and 304W contained mean

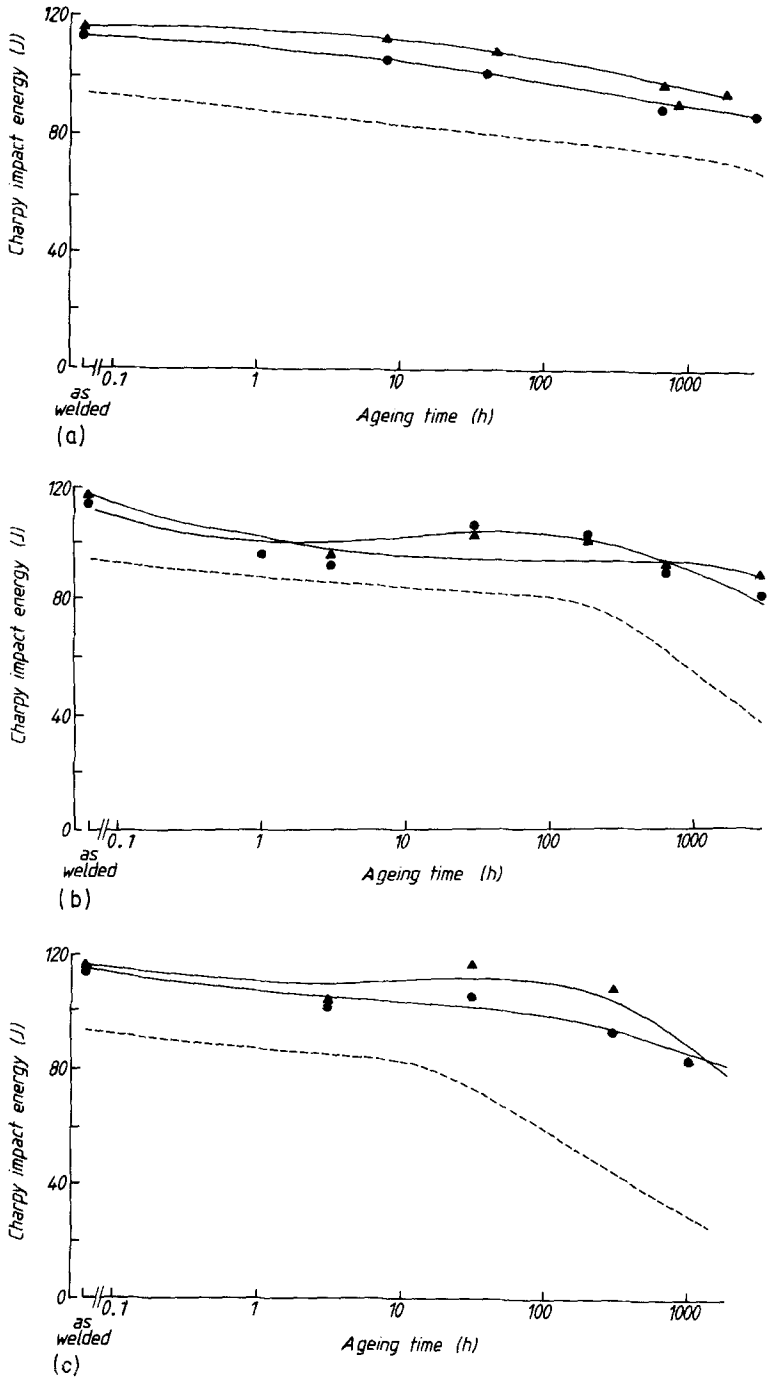

Figure 4 Effect of ageing at (a) 600, (b) 700 and (c) 800° C on room-temperature impact properties. (▲) 304 LW, (●) 304 W, (– – –) BW15.

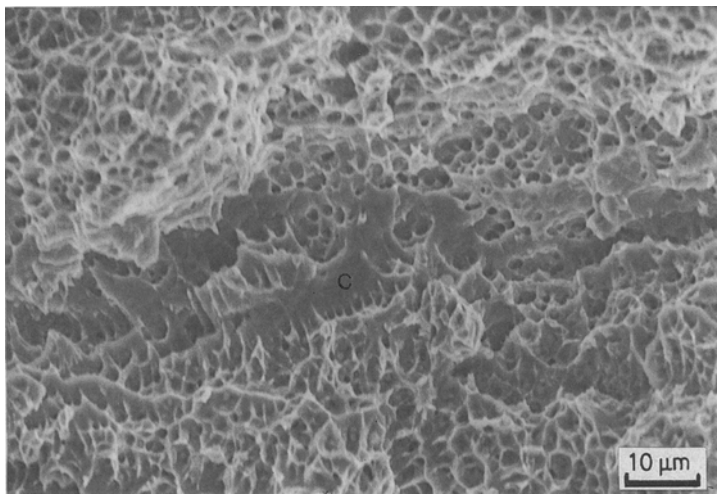

Figure 5 SEM micrograph of impact fracture surface showing small region of cleavage fracture (C) in 304 LW after 3000 h at 700° C.

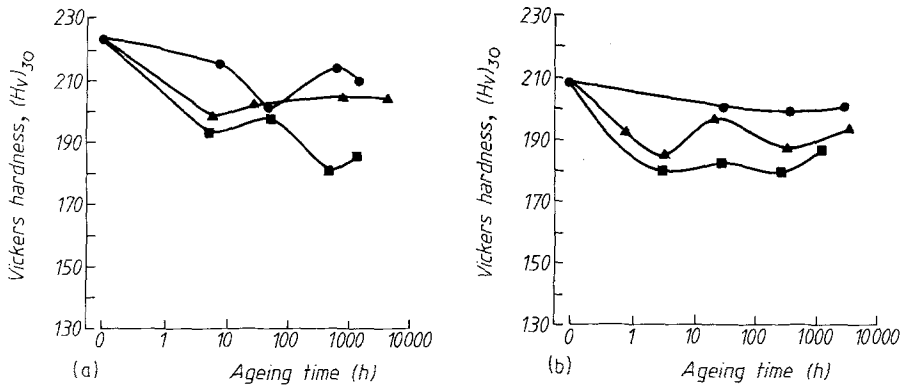

Figure 6 Effect of time and temperature on the hardness of (a) 304 LW, (b) 304 W. (●) 600° C, (▲) 700° C, (■) 800° C.

δ-ferrite levels of 4.6 and 4.7%, respectively. The distribution was characterized by columns of skeletal δ-ferrite aligned along the primary dendrite growth direction and parallel to the heat flow axis or columnar growth direction (Fig. 7). There was extensive interlocking of the secondary arms such that the δ-ferrite appeared as a semi-continuous network. This type of δ-ferrite morphology has been classified by David [8] as a vermicular δ-ferrite. Transmission electron microscope studies revealed the δ–γ boundaries to be devoid of any precipitation. This was further corroborated from X-ray diffraction data, obtained from the residue collected after the electrochemical dissolution of the austenite.

At the interpass boundaries, reheating induced by the multipass process resulted in the dissolution of the secondary dendrite arms and the appearance of a less continuous, globular δ-ferrite distribution (Fig. 7). The globular δ-ferrite still retains some directionality which is thought to be associated with the primary dendrite core.

3.5.2. Aged microstructure

3.5.2.1. Ageing at 600° C. In weld metals 304LW and 304W, after ageing at 600° C for 8 h, the δ-ferrite morphology was similar to that of the as-welded material but with some spheroidization of the secondary dendrite tips. After longer ageing times these changes became more pronounced, with the spheroidization and detachment of the secondary dendrite arms (Fig. 8). In 304W after ageing for 870 h, transmission electron microscopy revealed the presence of thin continuous films of $M_{23}C_6$ carbide along the δ–γ boundaries, (Fig. 9). In weld metal 304LW these carbide films were continuous, but after 3000 h these carbides showed some tendency to spheroidize and become discontinuous.

3.5.2.2. Ageing at 700 and 800° C. The changes in δ-ferrite morphology at 700° C were similar to those observed at 600° C, except for an increase in the rate of δ-ferrite dissolution (Fig. 10). In both 304LW and 304W, ageing resulted in the progressive dissolution of the δ-ferrite with the appearance of new austenite and $M_{23}C_6$ carbides. In 304LW, only small amounts of carbide precipitated at the δ–γ boundaries. Although these carbides were generally of a fine discontinuous type, occasional larger carbides were identified. However, in 304W extensive carbide precipitation occurred along the δ–γ boundaries (Fig. 11a). These carbides were observed to develop rapidly into δ-ferrite, adopting a Widmanstatten morphology [4]. After longer ageing times at 700° C, the carbides showed some tendency to spheroidize and become more discontinuous (Fig. 11b). At higher ageing temperatures these effects were more pronounced. After ageing times in excess of 3000 h at 700° C and 1000 h at 800° C, small quantities of intermetallic σ phase

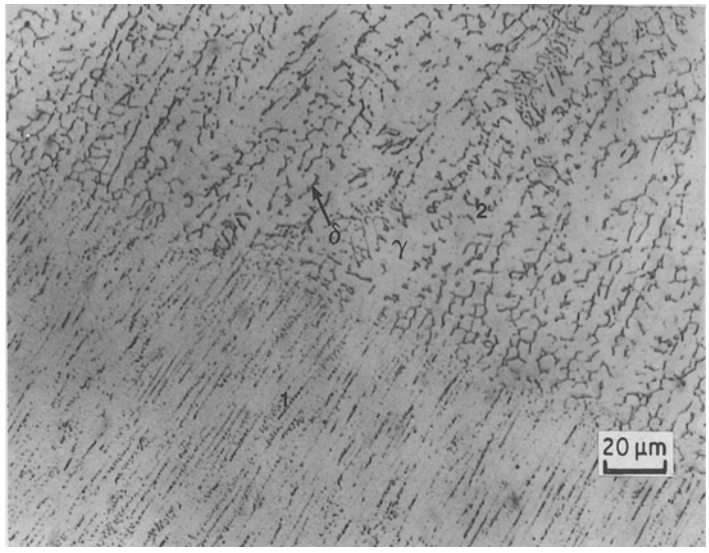

Figure 7 Optical micrograph showing change in δ-ferrite morphology across interpass boundary region in 304 W (as-welded).

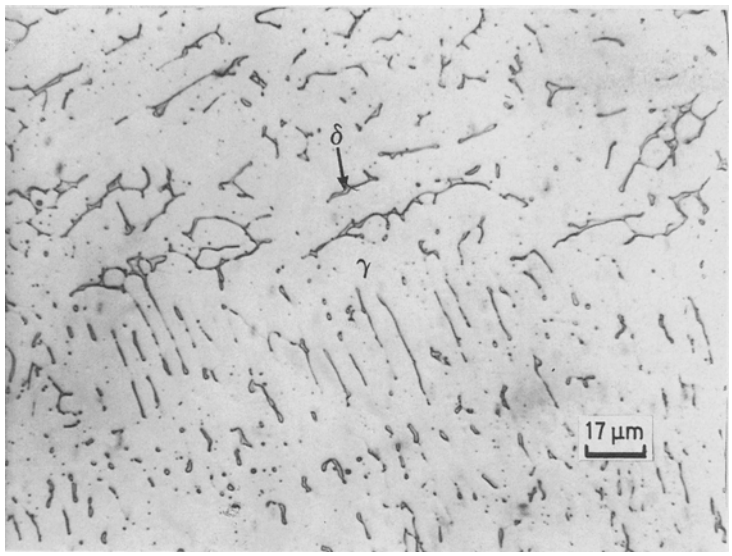

Figure 8 Optical micrograph showing the breakdown of the interlocking δ-ferrite structure in 304 LW after 800 h at 600° C.

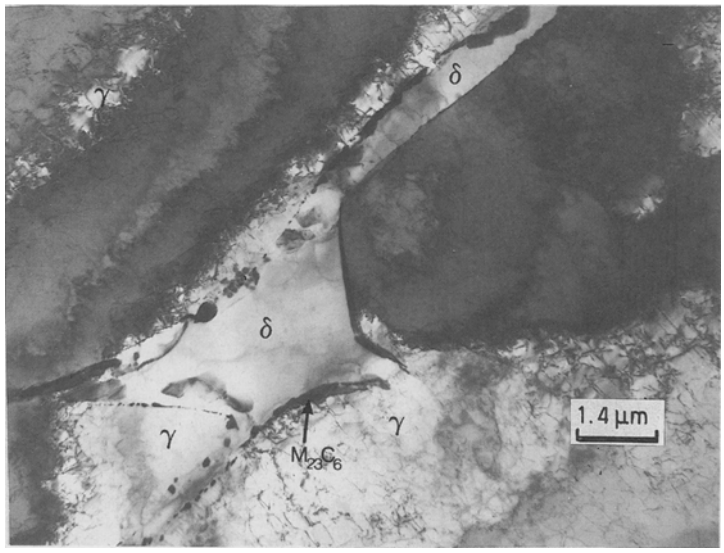

Figure 9 TEM micrograph showing semi-continuous films of $M_{23}C_6$ carbide at the δ–γ boundaries in 304 W after 870 h at 600° C.

precipitated in the δ-ferrite (Fig. 12). The intermetallics were typically 1 to 2 μm in size, discontinuous and highly spheroidized.

4. Discussion

In agreement with previous studies of duplex weld metals [7, 9, 10], it has been shown that the kinetics of δ-ferrite dissolution in the tungsten-containing deposits can be modelled using the Johnson–Mehl equation. Comparison of the δ-ferrite transformation curves for 304LW, 304W and BW15 indicate that the rates of δ-ferrite dissolution, in the tungsten-containing deposits, were significantly faster when compared with the standard 17Cr–8Ni–2Mo type. This implies that

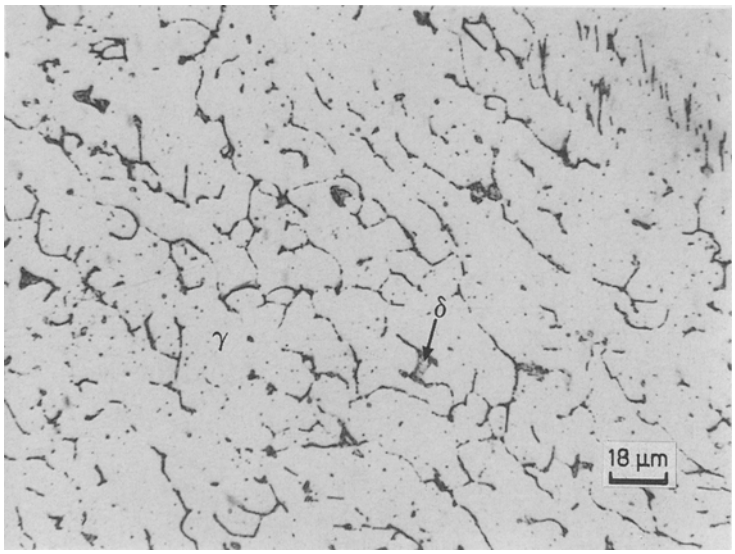

Figure 10 Optical micrograph showing the dissolution of the δ-ferrite in 304 W after 200 h at 700° C.

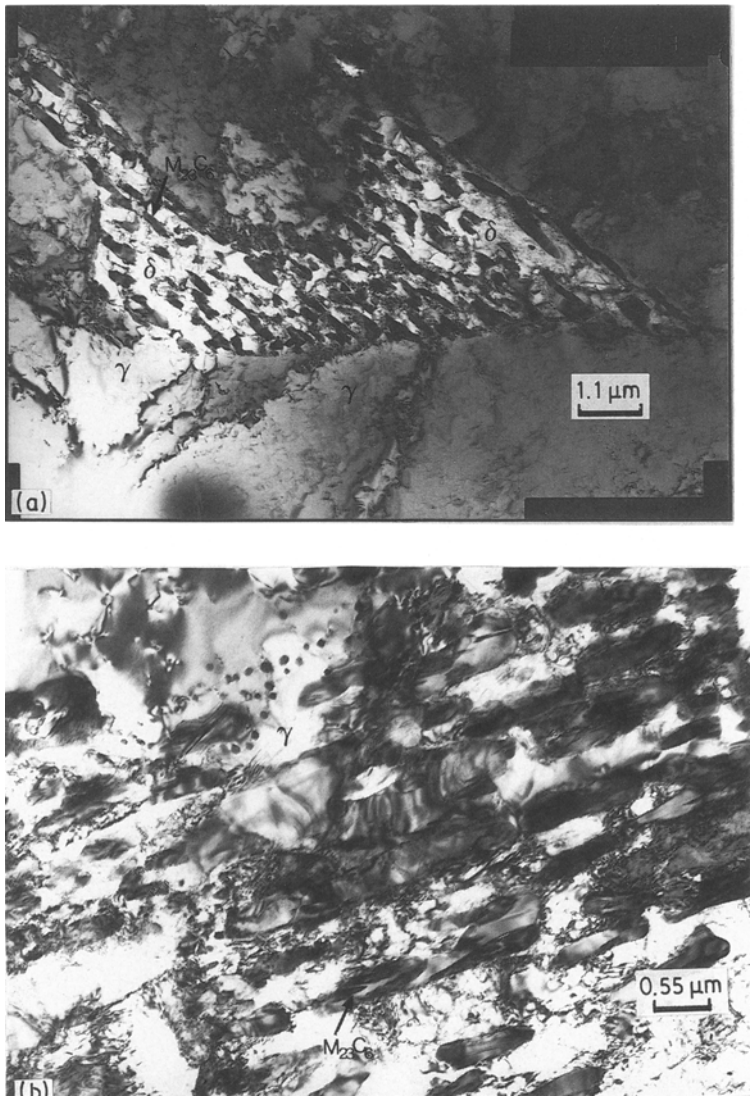

Figure 11 TEM micrographs of 304 W showing (a) the development of Widmanstatten $M_{23}C_6$ carbide in the δ-ferrite after 1 h at 700° C, and (b) spheroidizing $M_{23}C_6$ carbide after 100 h at 700° C.

the substitution of tungsten for molybdenum in 316 weld metal accelerates the rate of δ-ferrite dissolution. This effect was particularly pronounced at the higher ageing temperatures. The present studies have shown that within the temperature range of investigation, the activation energy for the dissolution of the δ-ferrite is probably not constant. This does not appear to be consistent with other studies of 17Cr–8Ni–2Mo and 19Cr–12Ni–3Mo type weld metals [7, 9, 10], which have reported the experimental data to be compatible with the Arrhenius equation (E = 315 to 400 J mol^{-1}). However, it seems likely that these values are in fact average activation energies and do not truly represent the kinetics of dissolution. This is because the transformation of the δ-ferrite can involve a complex multiphase reaction, with the preferred reaction $\delta \rightarrow \sigma + \gamma + M_{23}C_6$ at temperatures above 800° C and $\delta \rightarrow \gamma + M_{23}C_6 + \chi$ at temperatures below 650° C. Thus it

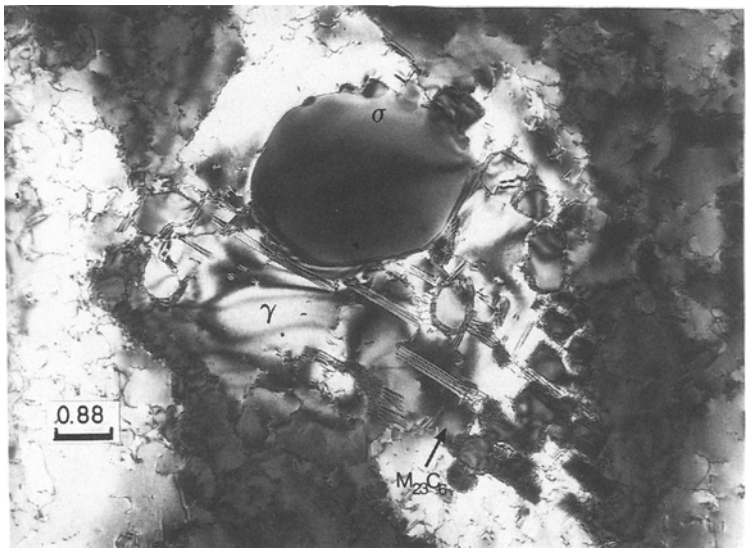

Figure 12 TEM micrograph showing small amounts of intermetallic phase in 304 W after 3000 h at 700° C.

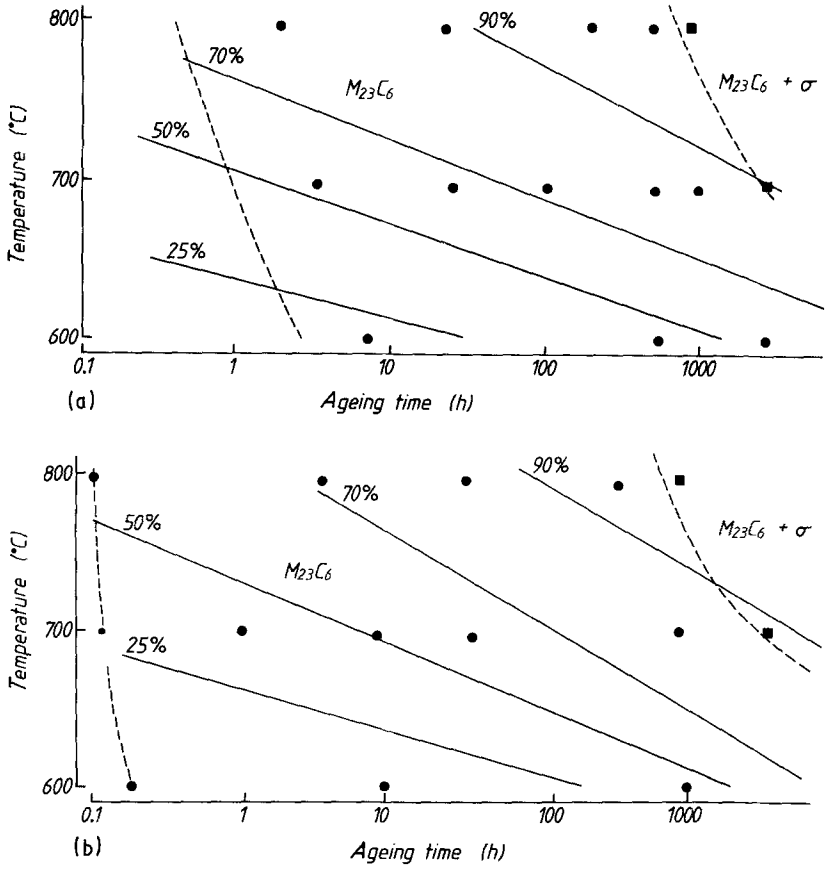

Figure 13 Time–temperature–precipitation diagrams for (a) 304 LW and (b) 304 W. (●) $M_{23}C_6$, (■) $M_{23}C_6 + \sigma$, (– – –) phase boundary, (——) percentage ferrite transformed.

is clear that the activation energy for the δ-ferrite transformation is dependent on a number of component activation energies, the relative contributions of which vary with temperature.

It has been suggested by Thomas and Keown [11] that the transformation equations derived from the Johnson–Mehl and Arrhenius models can be used to predict the δ-ferrite transformation behaviour under service conditions. However, from the above discussion it is likely that these transformation equations are inaccurate and that any attempt to extrapolate them to service temperatures will be subject to large errors. From X-ray diffraction studies in support of the ageing metallography, time–temperature–precipitation (TTP) diagrams have been constructed for weld metals 304LW and 304W (Figs 13a and b, respectively). In order to allow a direct comparison of the transformation behaviour in the deposits, Fig. 14 shows the TTP diagram for BW15 (17Cr–8Ni–2Mo type). A number of differences in transformation behaviour are apparent:

(a) The intermetallic boundaries in 304LW and 304W lie to the right of BW15, indicating a lower propensity for the formation of intermetallic σ phase.

(b) Within the ageing times and temperatures studied, the intermetallic χ phase did not precipitate in 304LW or 304W.

In addition to these differences, the diagrams further emphasize the high δ-ferrite transformation rates in 304LW and 304W compared with BW15. This implies that although the tungsten additions accelerate the

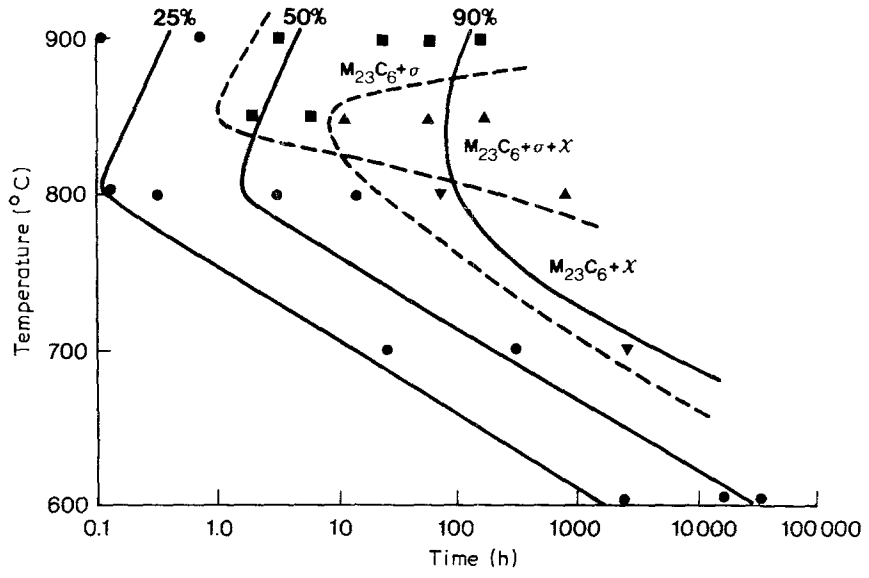

Figure 14 Time–temperature–precipitation diagram for BW15 (after Farrar [7]). Phases identified: (●) $M_{23}C_6$, (■) $M_{23}C_6 + \sigma$, (▼) $M_{23}C_6 + \chi$, (▲) $M_{23}C_6 + \sigma + \chi$, (——) percentage ferrite transformed.

rate of δ-ferrite dissolution, the additions inhibit the formation of intermetallic σ phase. This was further supported from the metallographic studies, which showed that 304LW and 304W transformed preferentially to austenite and $M_{23}C_6$ carbide. In addition, the impact tests showed that in weld metals 304LW and 304W, the impact toughness did not deteriorate significantly during ageing (Fig. 4). At all temperatures, the impact toughness values of the tungsten-containing deposits were consistently above that of the 17Cr–8Ni–2Mo deposit. The absence of the χ phase intermetallic in the tungsten-containing deposits appears to be consistent with studies by other workers. Leitnaker [12] has reported that the role of molybdenum was critical in controlling the formation of χ phase.

The present results suggest that the 304LW consumable is superior to BW15 in the aged condition. The 304 LW deposit contained only half the carbon level of BW15 but displayed a greater resistance to intermetallic formation. In addition, the lower carbon-containing deposits are known to be less susceptible to grain boundary sensitization. Only minimal carbide precipitation occurred in the 304LW deposit and the material would not be expected to be susceptible to this type of corrosive attack. It has also been shown that tungsten, like molybdenum, reduces the susceptibility to corrosion by extending the passive potential range and lowering the passive current density [13].

The present results suggest that 304LW has the potential for the development into a welding consumable with

(a) enhanced high temperature properties, and

(b) properties which will not deteriorate significantly with time or temperature.

Further work is at present being undertaken to evaluate the mechanical and high-temperature properties of this material. However, the effect of tungsten and molybdenum on the creep rupture strength of austenite are known to be similar [14], and consequently it is expected that the mechanical properties will be at least equivalent to those of the 17Cr–8Ni–2Mo weld metal.

5. Conclusions

1. In the temperature range 600 to 800° C, the δ-ferrite transformation process can be modelled using the Johnson–Mehl equation.

2. The activation energy characterizing the dissolution of the δ-ferrite was temperature-dependent.

3. On ageing in the temperature range 700 to 800° C, the δ-ferrite rapidly transformed to new austenite and $M_{23}C_6$ carbides. Small quantities of intermetallic σ phase were identified only after ageing in excess of 1000 h at 800° C and 3000 h at 700° C.

4. The substitution of tungsten for molybdenum inhibited the formation of intermetallic χ phase.

5. Within the ageing times and temperatures studied, the tungsten-containing deposits exhibited superior impact properties to the standard 17Cr–8Ni–2Mo deposit.

Acknowledgements

This work was carried out in conjunction with Marchwood Engineering laboratories (CEGB) and the authors are grateful to the laboratory manager for the provision of technical facilities. The authors also wish to thank Mr J. Weaving for performing the X-ray diffraction analysis. Acknowledgement is made of financial support by SERC CASE Award SB101 for one of the authors (J.J.S).

References

1. R. G. BERGGREN, N. C. COLE and G. M. GOODWIN, *Welding J. Res. Suppl.* **56** (1978) 167s.
2. C. R. BRINKMAN, V. K. SIKKA and R. G. KING, *Nucl. Technol.* **33** (1977) 76.
3. R. A. FARRAR, *J. Mater. Sci.* **20** (1985) 4215.
4. J. J. SMITH, PhD thesis, Southampton University (1989).
5. J. WEGRZYN and A. KLIMPEL, *Welding J. Res. Suppl.* **60** (1981) 1s.
6. F. C. HULL, *ibid.* **46** (1967) 399s.
7. R. A. FARRAR, C. HUELIN and R. G. THOMAS, *J. Mater. Sci.* **20** (1985) 2828.
8. S. A. DAVID, *Welding J. Res. Suppl.* **61** (1984) 63s.
9. R. G. THOMAS and D. YAPP, CEGB Report R/M/R273 (1979).
10. R. A. FARRAR and R. G. THOMAS, CEGB Report TPRD/M/1251/N82 (1982).
11. R. G. THOMAS and S. R. KEOWN, CEGB Report RD/M/R312 (1981).
12. J. LEITNAKER, *Welding J. Res. Suppl.* **62** (1982) 9s.
13. A. J. SEDRIKS, in Proceedings of "Stainless Steel' 84", Goteborg, 1984 (Institute of Metals, London, 1985) p. 223.
14. T. SHINODA, T. MATSUO, R. TANAKA, in Conference Publication No. 13 (Institute of Mechanical Engineers, London, 1973).

Received 30 January
and accepted 11 May 1989